Fracture Evaluation of Multi-layered Precast Reinforced Geopolymer-Concrete Composite Beams by Incorporating Acoustic Emission into Mechanical Analysis

Navid Ranjbar[1,*], Arash Behnia[2*], Hwa Kian Chai[3], Jhonson Alengaram[4], Mohd Zamin Jumaat[4]

[1] *Department of Civil Engineering, Engineering Faculty, Shiraz University, Iran*

[2] *Department of Civil Engineering, School of Engineering, Monash University*

[3] *Infrastructure and Environment Institute, School of Engineering, the University of Edinburg, United Kingdom*

[4] *Department of Civil Engineering, Engineering Faculty, University of Malaya, Malaysia*

Keywords: Multilayers beam; Composite; Geopolymer; Reinforced concrete beam; Fly ash; Acoustic emission; Damage, horizontal shear crack.

Abstract

In this study, a multi-layered steel reinforced composite beams which are composed of geopolymer concrete section at tensile zone and Portland cement based concrete at compression are investigated. The beams were tested to failure to compare the toughness, post peak behaviour and failure mode based on the variation of the depth of layers. The mechanical analysis incorporated into acoustic emission technique showed that the geopolymer beam endured more deflection than the ordinary Portland cement based beams, however their ultimate load carrying capacities were quite similar. Further, the composite beams, resulted in transition of failure mode of shear to a flexural.

---

[*] *Corresponding authors: arash.behnia@monash.edu, n.ranjbar@shirazu.ac.ir*

1. Introduction

Precast reinforced concrete elements have been extensively used in construction over the past decades due to its time and cost effectiveness and higher quality of the products [1]. However, the integrity of components is a main concern in precast structures. To increase the efficiency of the construction, partially precast beams is mostly used so that combination of precast and in situ sections. As a result, the integrity of structure is increased in comparison to those of fully precast systems, while it becomes more economical, faster and easier compare with in situ construction [2]. Partially precast beams are comprised of a section which is fabricated in factory having a part of reinforcements out from the concrete body; this section is placed as the tensile zone (bottom) of the beam. Such sections are transferred to the site and connected to other members using in-situ construction to make a uniform structure. In this system, the precast section are designed to assemble fast and to carry the further loads from in-situ casting. Figure 1 shows an example of such beams.

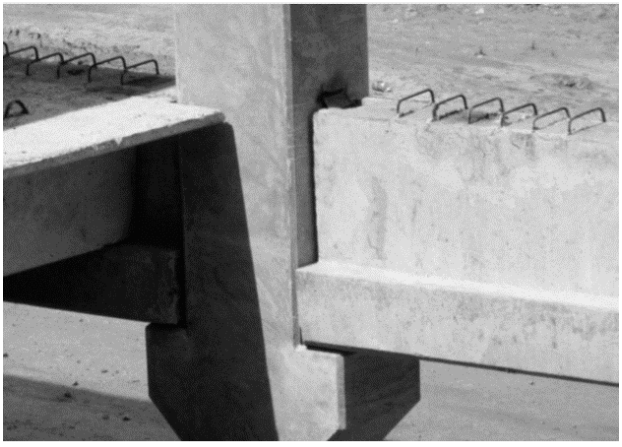

Fig. 1. Application of multi-layers composite inverted T-beam [3].

Geopolymer are inorganic aluminosilicate polymeric materials with near ambient curing and hardening temperatures [4]. They were first introduced with the industrial development of new binder in 1972 by Davidovits. Due to their superior properties of high early strength compare with Portland cement, geopolymers are seen as prospective construction materials for precast industry [5-9]. These materials are used to fabricate several precast elements such as retaining walls, sewer pipes, roofing tile, footpaths, pavement, water tanks, precast bridge decks, precast beams, slabs, panels (Melton Library, Melbourne, Australia) and even full scale building(Global Change Institute - University of Queensland) [10-12].

Despite numerous potential geopolymer applications, there are some drawbacks in its widespread utilization and commercialization. As a novel structural binder, the main issue is the compliance of design procedure with the current standards which mostly consider the specific physicochemical properties of Portland cement products. However, alkali-activated concretes are ideally suited to be regulated through a performance-based approach, as per ASTM C1157, which shows the prospective potential for further developments of non-conventional binder systems [12-14]. Furthermore, the promising prefabrication potential of geopolymer paves the way for its industrialization [15].

This research aims to investigate the differences between the performances of ordinary Portland cement (OPC) and geopolymer (GPC) reinforced concrete beams and the effects caused by replacement of GPC in the tensile zone of high strength Portland cement based reinforced concrete beams subjected to a three point bending load from the aspects of specimen ductility, energy absorption, mode of damage and failure. Geopeolymer concrete was replaced to the tensile zone of the beam because of its great potential in high early strength which makes it preferable binder for precast industry. Besides, the top layer of the composite beams were

fabricated by OPC which is the conventional material for in-situ constraction. The results demonstrate that the multi-layer geopolymer composite beams had higher degree of toughness and deformation than the OPC without adverse effects in its maximum load carrying capacity; moreover, the shear based mode of damage in OPC beam changed to a flexural mode in the geopolymer and composite beams.

2. Summary of experimental investigation

2.1. Materials characterization

The batches of low calcium FA (class F) and Portland cement used in this research were collected from Lafarge Malayan Cement Bhd-Malaysia and Tasek Corporation Berhad- Malaysia with the specific gravity of 2.18 and 3.15, respectively. Particle size distributions of fly ash and cement were measured with (Mastersizer, Malvern Instruments, Malvern, UK) and results are shown in Figure 2. The chemical composition of the materials as determined by X-ray florescence by PANalytical Axios mAX (Netherlands) instrument and LOI value are provided in Table 1.

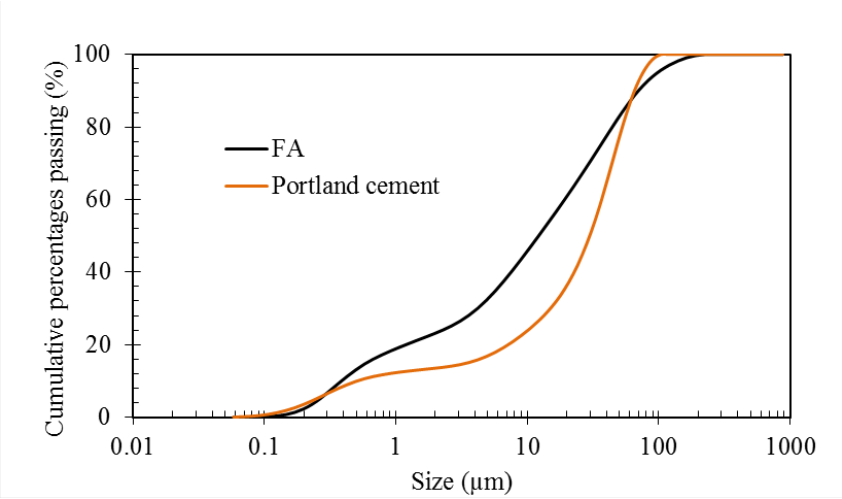

Fig. 2. Particle size distribution of the fly ash and Portland cement.

Table 1. XRF analysis of the Fly ash and Portland cement

Oxide composition	Fly ash (%)	Portland cement (%)
SiO_2	75.76	16.68
Al_2O_3	15.86	4.41
Fe_2O_3	3.90	3.64
K_2O	1.14	0.37
TiO_2	0.97	0.17
CaO	0.95	68.36
SO_3	0.35	4.80
MgO	0.26	1.29
P_2O_5	0.21	0.05
Na_2O	0.16	-
ZrO_2	0.13	-
MnO	0.06	0.10

Local fine aggregate were prepared with the minimum and maximum particle size limited to 300 μm and 4.75mm, respectively. The coarse aggregate was obtained from Batu Tiga Quarry Sdn Bhd (YTL), Malaysia with a maximum particle size of 10mm.

To activate the precursor, a mixture of sodium silicate solution (Na_2SiO_3) and sodium hydroxide (NaOH) pellets with a purity of 99% has been prepared beforehand. The NaOH pellets were obtained from Merck (Germany) and the Na_2SiO_3 solution (SiO_2=12%, Na_2O=30%) from PC Laboratory Reagent.

2.2. Geopolymer and Portland cement concrete preparation

The OPC was prepared by dry mixing of fine and coarse aggregate together with cement for 2 minutes by a concrete drum mixer with the capacity of 0.3 m^3, to make a uniform particle distribution in dry stage. The coarse to fine aggregate ratio was kept at 1.5 for all the specimens. 10 more minutes of mixing with the addition of water to keep the water-binder ratio to 0.26.

MASTERGLENIUM ACE 8388 (GLENIUM ACE 388RM) superplasticizer was used at 0.02 wt% of the binder to provide the workable mix. The concrete layer was poured in to the molds immediately after the mixing and vibrated with a manual vibrator to remove the air bubbles and to fill the space between reinforcements. The thickness of the layer varied between 150, 125 and 100 mm. The half casted beam was cured for 24 hours in ambient condition with an average temperature and humidity of 28 °C and 70%, respectively.

The alkali activator solution was prepared by mixing 16 molar NaOH with Na_2SiO_3 solution with Na_2SiO_3 to NaOH ratio of 2.5. The activator to fly ash ratio was kept at 0.5 for all the specimens. First, dry sand, gravel and fly ash were mixed together for 2 minutes followed by addition of 0.15 wt% of the binder, tap water and mixing for next 3 minutes. Alkali activator was gradually added to the mixture and mixed for another 5 minutes. The GPC was immediately poured into the molds and compacted to make sure it is passed through the reinforcements and reduced the vacant space and porosity. It should be noted that due to low workability and inherent cohesiveness of the GPC, a vertical mixer was selected to avoid accumulation of the concrete at the wall of the mixer and poor mixing condition. The beams were kept in 65 °C oven for 24 hours and afterward dismantled and cured in ambient condition until the day of testing. Figures 3.a--c show the casting procedure of composite beams and different layers preparation including OPC layer, GPC layer, and final composite product, respectively.

Fig. 3. Casting of different layers and final beam products.

2.3. Geometry and reinforcement

A set of one OPC, one GPC and three multi-layer beam specimens were fabricated. Each beam. The mechanical properties of the OPC and GPC at 28th day are obtained using the average of at least 6 specimens and shown in Table 2. 100 mm cubes are used for compressive strength and 100x200 mm cylindrical specimens are used to determine the splitting and Young's modulus.. Noteworthy, the tensile to compressive strength ratio of GPC is higher than that of OPC; therefore, for a similar flexural strength, the compressive strength of concrete would be higher than geopolymers [13, 16].

Table 2. Mechanical properties of the Portland cement based and geopolymer concrete.

	Compressive strength, f_c (MPa)	Tensile strength*, f_{ct} (MPa)	Young's modulus, E (GPa)
Geopolymer concrete	42±3	5.2±0.3	22.4±1
High strength concrete	88±5	5.5±0.2	40.5+2

*Similar tensile strength is considered for the OPC and GPC since the tensile zone of the beams are replaced.

All the composite beams having a rectangular cross-section with b = 125 mm width, H = 200 mm height and L = 1000 mm length. The bottom layer of beams was fabricated by geopolymer concrete with varying depth of 0, 50, 75, 100 and 200 mm in specimens B1 to B5, respectively, and the upper layer was filled with OPC. The beams were reinforced with two flexural high-tensile strength, hot-rolled, deformed steel bars with a diameter of 10 mm and a yield strength of about 670 MPa with a distance of C-C 65 mm which bent upward to provide a support for stirrups with the curtailment of 300mm; and shear reinforcement mild steel with a diameter of 6 mm and a yield strength of approximately 350 MPa at a spacing of 100mm for distance of 300 mm from each end of the beam. Details of the multilayer beams are presented in Figure 4.

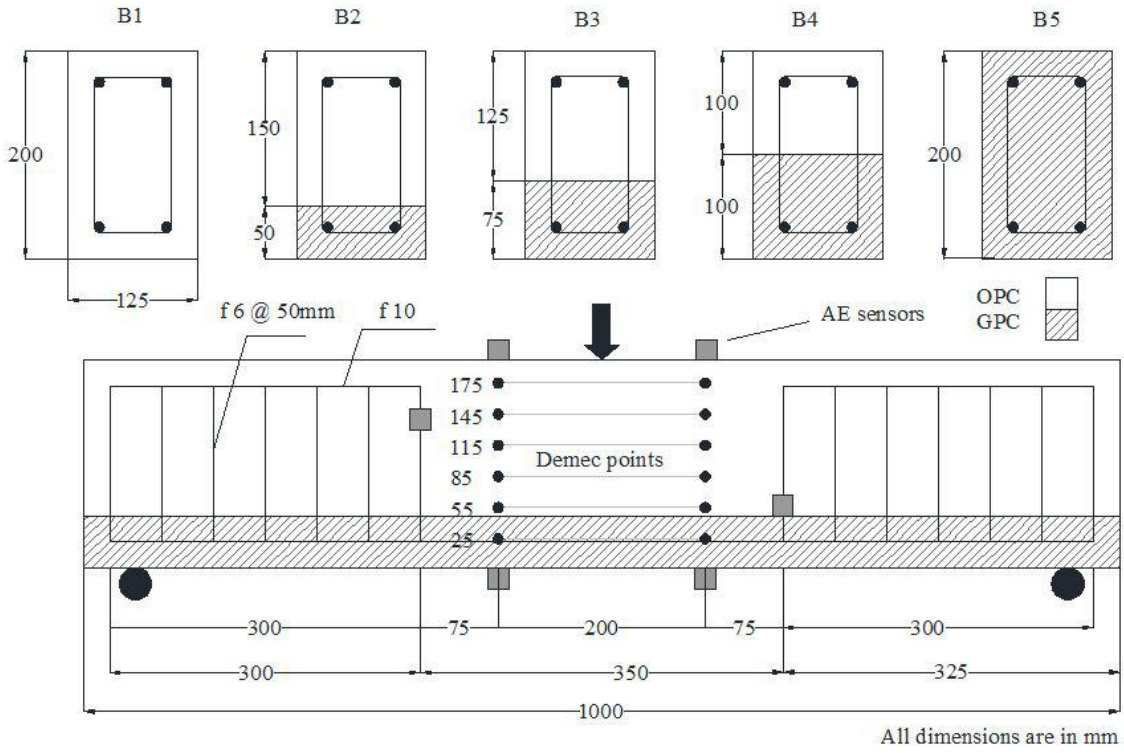

Fig. 4. Geometry of the multilayers steel reinforced GPC/OPC composite beams.

2.4. Testing methods and instrumentation

2.4.1. Mechanical and experiment setup

The multilayers beams were tested using three point bending load with the rate of 0.5mm/min however there was a stop at each 5 kN for 4 minutes to record the crack propagation and neutral axis variations. The load was applied continuously after the beam yielded until the ultimate failure. The experiments were carried out on an INSTRON SATEC 600 KN universal testing machine. The strains in the main reinforcements were measured by electrical resistance strain gauges and recorded through a data logger. Moreover, linear voltage differential transducers (LVDT) were placed under the beam mid-span to measure the vertical deflection. The nominal toughness of beams were measured as the area under the load-deflection curve of each specimen and presented relative to the OPC beam.

Demec points were fixed at the middle of the beams as shown in Figure 4. The variation of strain and depth of the neutral axis of the beam specimens over time was measured by using of Mitutoyo Absolute Digimatic Indicator ID-C112B apparatus with the range and resolution of 12.7 mm and 0.001 mm, respectively. The strains at the middle of the flexural reinforcements were measured by electrical resistance strain gauges and recorded through a data logger.

2.4.2. AE measurement and instrumentation

Acoustic emission (AE) sensors were incorporated into mechanical measuring process. AE is defined as the propagation of elastic waves due to the release of localized internal energy such as micro-fracturing in the material [17, 18]. The source of AE activities is irreversible changes in the structure such as crack expansion. Procedure of using AE is to detect the released strain

energy generated from growing cracks using sensors [19, 20]. To monitor the cracks and event distribution patterns a conventional AE event 2D localization technique was performed. The AE measurement system (by Mistras Group Inc.) consisted of PCI-2 data acquisition boards that accommodate a total of six AE sensors and a windows-based AE data operation program known as AEwin was utilized. A total of six AE sensors was mounted on the specimens. AE sensors used this study have a resonant excitation frequency of 60 kHz (R6l in the measurements, the sampling rate was set to 2 MHz, with the pre trigger set to 250,000 μs. The hit definition time (HDT), hit lockout time (HLT), and wave velocity were configured as 2000 μs, 300 μs and 3900 m/s, respectively. To eliminate electrical and mechanical noise, the threshold level was set at 45 dB. It is noteworthy, a pencil lead break test and Q value analysis was conducted to obtain the signal velocities and amplitude attenuation level.

3. Results and discussion

3.1. Load-deflection relationship

The characteristics of reinforced concrete beams under flexural loading can be roughly categorized in three different stages: uncracked elastic, crack propagation and plastic deformation. After formation of the first macro-crack, the cracked beam shows a visible change in load-deflection slope which is an indication of the onset of inelastic response stage. The inelastic response of the beams is due to three major material effects including concrete cracking, reinforcement yielding and concrete crushing [21].

The load–displacement curves of the beams are shown in Figure 5. The deflection of all the beams was increased linearly proportional to the load upon initiation of first visible crack. It is

noteworthy, although GPC had significantly lower compressive strength than OPC, for both the formation of first visible crack occurred almost at the similar loading ratio at 20% of ultimate load. This could be attributed to the differences in characteristic of the corresponding materials which the tensile to compressive strength ratio is higher for GPS than that of OPC [13, 16]. However, onset of profuse cracking was an indication of non-linearity for all the beams until yielding point. Noteworthy, although all the beams had almost similar yielding points, they exhibited different behaviors. The yielding point of the GPC beam emerged gradually, whereas the OPC beam reached its yielding stage in a rather sharp trend [22]. The point of interest is that both the GPC and OPC beams had approximately the same load carrying capacity while the GPC beam deflected about twofold of what the OPC beam showed at the failure point, although the compressive strength of the geopolymer was about half of the Portland cement based concrete. The higher deflection of GPC compares with OPC at the a similar load capacity was also observed by Andalib et.al [22].

On the other hand, all the composite beams benefited from the composite action of geopolymer with high tensile strength and concrete with high compressive strength which retarded the occurrence of first visible crack and slightly higher load carrying capacity. In addition, all of the composite beams experienced an improved post yielding response relative to that of OPC beam, however their stiffness was about similar. This might be attributed to the higher bond strength of geopolymer to steel reinforcement than concrete to steel [23-25].

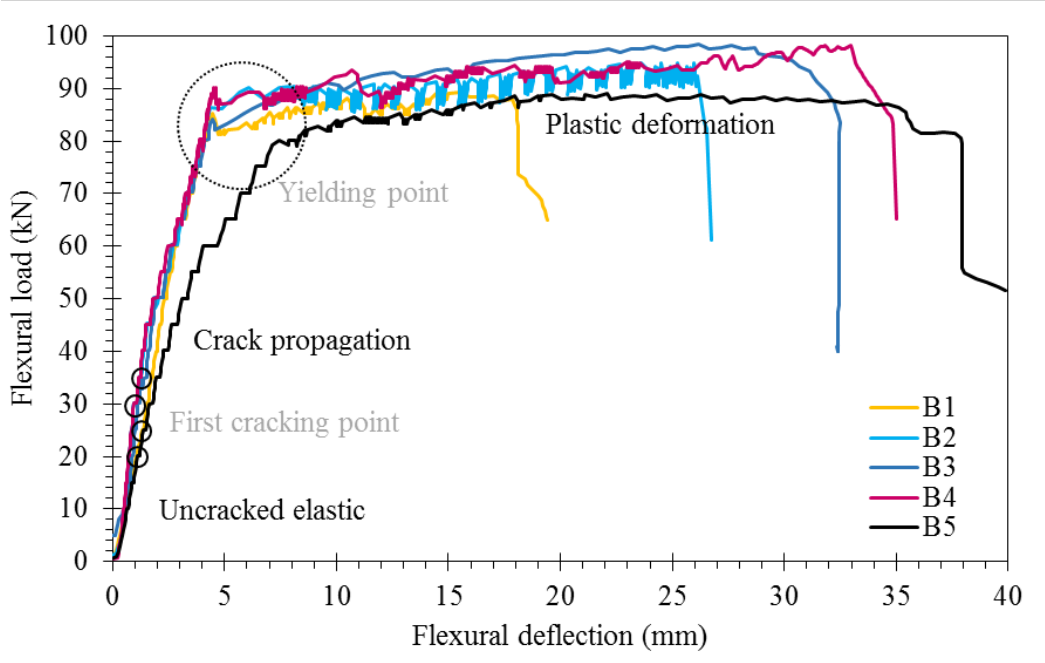

Fig. 5. Load-deflection curves of multilayer GPC/OPC steel reinforced concrete beams.

Figure 6 shows the total toughness and ultimate strength of the beam specimens. As observed, by increasing the height of GPC layer to 50% of the whole section, the toughness of the beam increases significantly while further increment did not have salient influence on toughness mechanism. The same trends were observed for the ultimate load carrying capacity of the composite beams although 100% replacement of the OPC with GPC resulted in strength loss to the certain load that carried by OPC specimens. The composite beams showed higher load carrying capacity than either geopolymer or concrete beams.

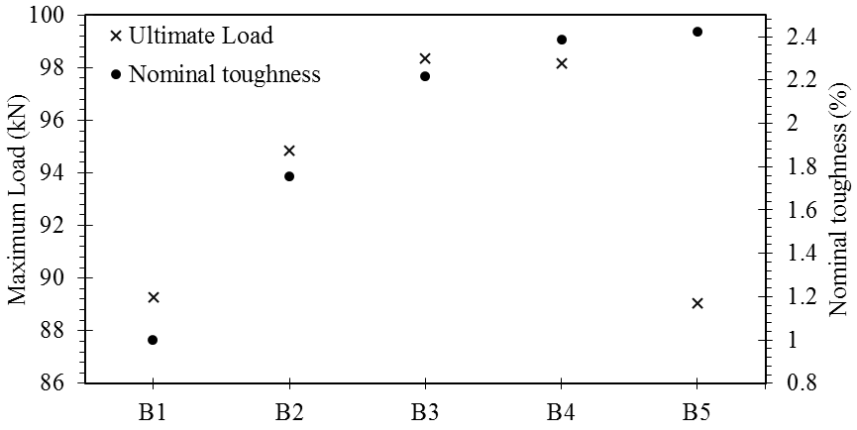

Fig. 6. Maximum load capacity and nominal toughness of the geopolymer composite beams.

3.2. Failure mode and crack patterns

The load was increased until the failure of the beam and the crack propagation was recorded continuously up to trigger of yielding point where the beams started to experience large deflection though carrying a small amount of load. The crack distribution of the beams is shown in Figure 7. The first cracks were detected at the flexural zone of the beams and summarized in Table 3. The first crack of concrete beam happened at 25 kN while it decreased to 20 kN for the geopolymer specimen; this value was increased significantly for composite beams. According to the structure of the beams, their crack distribution patterns were independent of the material properties and could be categorized into uniform and multi-layer beams. As observed in Figures 7.a and 7.b, once a flexural crack was formed at a uniform specimen, it had potential to extend upward during the loading process. However, formation of new cracks or extension of the old ones after 60 kN was higher in the GPC than OPC. However different mechanisms were observed in the composite beams as shown in Figure 7.c. In these specimens, the first crack formed in geopolymer layer and extended through the concrete layer until the load of about 55

kN; at this load a horizontal crack formed at the contact surface of the OPC and GPC, as observed in Figures 7.d-e. The propogation of horizontal shear crack at the interface reflects the distribution of shear along the sections [26]. Further load increment resulted in formation of new cracks in geopolymer layer which merely could extend until the contact surface and deflect horizontally. In other words, further crack formation was limited to the geopolymer layer. As an illustration, Figures 7.e-f shows the crack pattern for the composite beam B4. In addition, considering the crack length in Table 3, the ratio of crack length before and after 60 kN decreased when the height of geopolymer layer was increased. This result implies that the rate of crack propagation and energy absorption at higher load is higher in GPC compare with OPC beam.

Figure 7.d and e show the presence of horizontal shear cracks at either support or through the axis of B2 and B3, respectively. However the presence of horizontal shear cracks was not recorded along the axis of B4, just some cracks formed at the end of the beams at a similar load, 55 kN, and therefore the total crack length was reduced in this specimen.

Table 3. Crack properties of the beams

Specimens	Depth of GPC layer (mm)	First crack Load (kN)	First crack length (cm)	Crack length (cm)			
				Load ≤60kN (cm)	Load>60kN (cm)	Total crack length until yielding (cm)	Before/after 60kN (cm)
B1	0	25	7	75	13	88	5.8
B2	50	30	12.5	89	33	122	2.7
B3	75	35	13	104	58	162	1.8
B4	100	30	9	76	40	116	1.9
B5	200	20	7	81	63	144	1.3

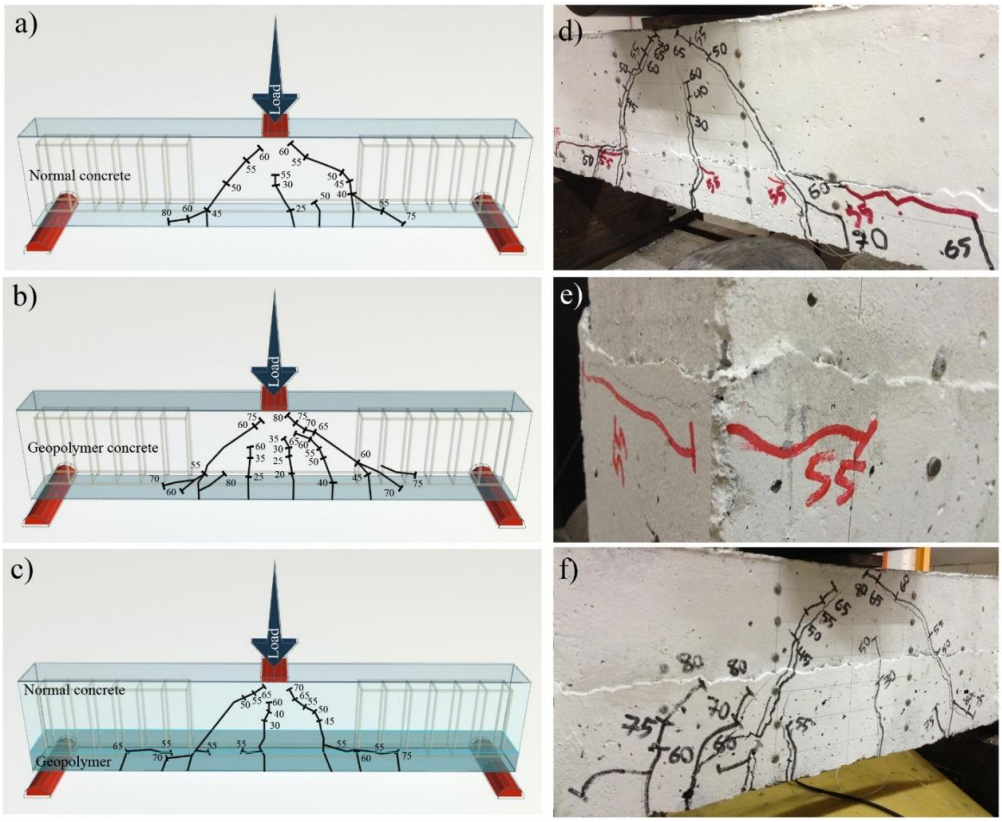

Fig. 7. Scheme of Crack patterns in a) OPC beam, b) GPC beam, c) composite beam-B2, d) experimental crack pattern of B2, e) horizontal shear force at the end of the B3, f) crack pattern of B4.

3.3. Variation of neutral axis

Strain variation along the height of beam section over load, Figure 8, shows the elastic and cracking stage of the specimens. As can be observed, formation of the first crack was noticed in both the OPC and composite beams by the deflection of concrete strain trend at the tensile zone which is manifested by the positive strain on the figures. Further loading resulted in movement of neutral axis upward with a high rate as expected for OPC beam. This mechanism was different in GPC specimen for which the trend of strain variation was gradual without any significant

variation. Interestingly, the compressive and tensile strain was approximately symmetric on cracking stage that shows the neutral axis of the beam was positioned at the middle of the section during the loading.

Considering the above description it can be noted that the depth of compressive block at cracking stage for GPC was higher than that obtained for either OPC or composite beams.

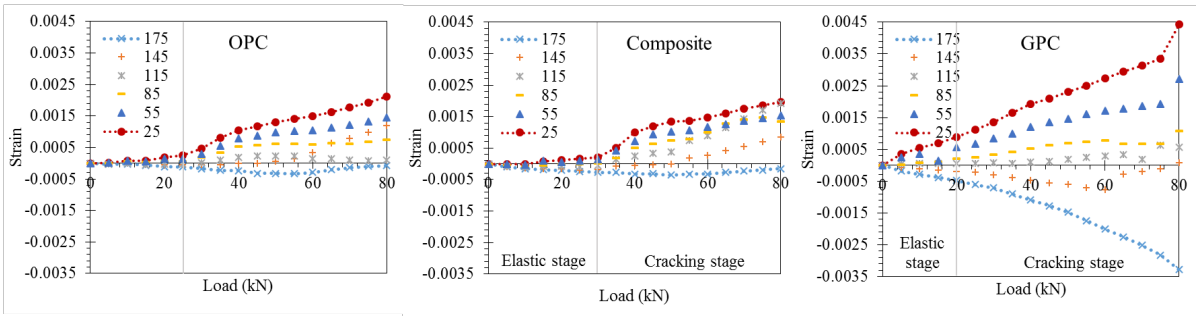

Fig. 8. Strain variation along the depth of the section over load. The legend shows the location of demec-points according to the Figure.4.

3.4. Damage localization by AE

Visual inspection and observation merely allows to capture those events emerging and taking place on the surface of beams, whereas cracks and events in concrete beams might be triggered beforehand the onset of first visible crack. Furthermore, during crack localization stage AE technique may reveal the location of prevailing interior and exterior damages. Based on the principle of arrival time difference between sensors, 2D conventional AE hypocenter localization analysis was performed to record the event localization analysis for concrete, geopolymer, and composite beams, presented in Figure 9. It should be noted that to highlight the density of event concentration in a comparative manner among the specimens a unified ratio of image smoothing

by benchmarking normal concrete beams against the other specimens was applied so that the better visualization could be achieved by eliminating scattered events distributed all over the beam length. As observed, the maximum number of AE events occurred for OPC specimen in a smaller range of length concentrating in the tensile zone, whereas GPC events with considerably lower number of events cover the larger area of beam. Composite beam had slightly lower frequency of AE event occurrence while pertinent AE events could cover a large area of the beam. Particularly, some AE events occurred associated with the cracking in contacting layer. This phenomena and the event distribution pattern can be correlated to the plasticity properties of material. As the brittleness of material increased the number of occurrence of AE events increased and consequently higher level of AE energy was obtained [18]. Therefore, GPC beam with higher plastic properties exhibited ductile behavior which was highlighted with fewer AE signals with total lower AE energy prior to peak load, whereas concrete beams suffered with many strong AE events prior to peak load. It is noteworthy that most AE signals and AE energy were associated with the post peak region of geopolymer and composite beam in contrast to concrete beam. In other words GPC and composite beams had higher rate of increase in crack length compared to the OPC specimens. However, it is completely visible that for composite and geopolymer concrete under flexural loading higher portion of beam elements were contributing in load carrying capacity with regard to scattered AE event along the entire length of the beams.

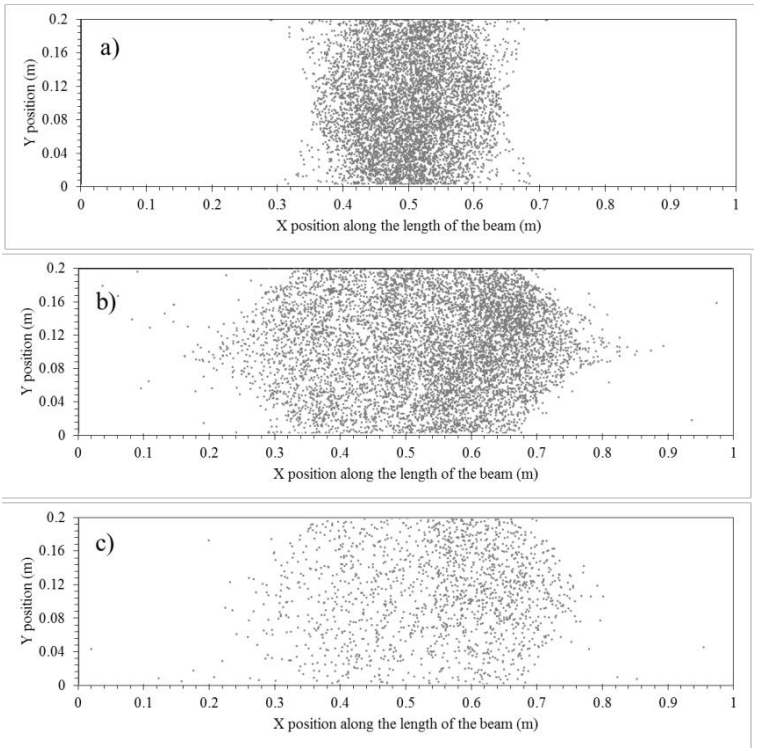

Fig. 9. 2D AE event localization of the a) OPC, b) Composite, c) GPC beam.

Figure 10 depicts the results of AE-events plotted versus the length of the OPC, composite, and GPC beam specimens. It is notable that the width over which the AE events took place is directly related to the size of fracture and damage zones. It can be inferred that composite and GPC beams possess larger width of fracture and damage zone which can be attributed to the ductile and plastic characteristics of the geopolymer concrete. According to the width of fracture (W_F) and damage (W_D) zones using the methods proposed by Haidar [27] and Rossi [28]. The fracture process zone can be referred as the intermediate space between cracked and uncracked portion. This region is defined as the Fracture Process Zone (FPZ). FPZ consists of micro cracks which are minute individual cracks that are situated nearer to crack tip. As the crack propagates these

micro cracks merge and becomes a single structure to give continuity to the already existing crack. This region called damage zone

The fracture process zone can be estimated by drawing a line at 20% of N_{max}, where N_{max} is the maximum number of AE events shown in Y-axis; and the line at 50% of N_{max} determine the width of damage zone, respectively [27, 28]. Accordingly, composite beam and concrete beams with 435mm and 225mm had maximum and minimum width of fracture zones, respectively.

.

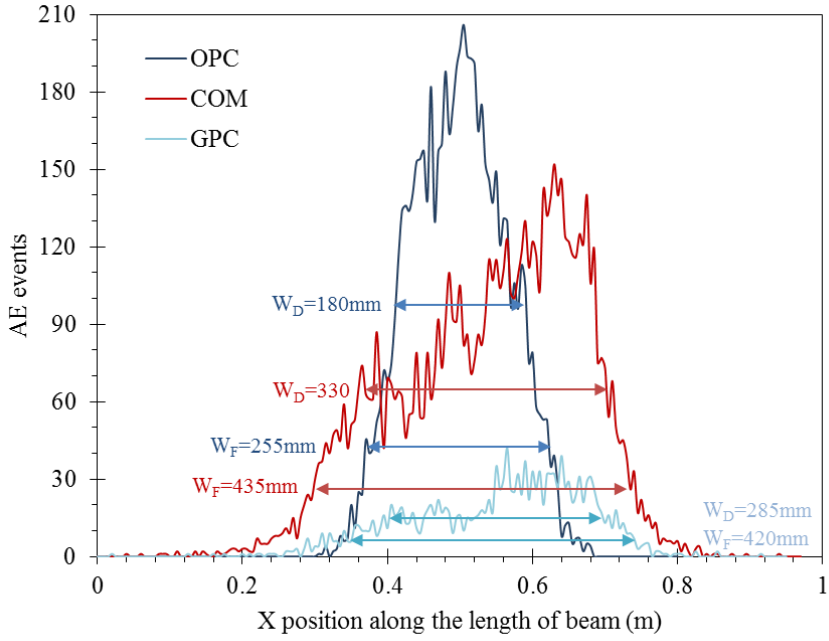

Fig. 10. AE-events versus specimen length.

3.5. Type of failure and nature of damage source by incorporating AE into mechanical results

RA (Rise time/Amplitude) and Average frequency were used to distinguish tensile cracking from shear cracking during fracture [17, 18, 27]. Indeed, different fracture modes produce different types of acoustic emission signals with varying frequency ranges and waveforms [18, 27, 30]. Therefore, differences in emitted signals are attributed to the wave modes which are excited by different types of cracks or damage. In general, flexural failure accompanied by tensile cracks result in a transient or short-lived burst volumetric change inside the material that makes the released energy convert to longitudinal/dilatational (p-wave) wave. Therefore, most excited pulses consist of longitudinal waves with larger amplitude which are subsequently faster than any other excited types that produce shorter rise time signals. On the other hand, shear is principally accompanied by shear cracks in which most of the energy is transmitted to shear/ distortional waves (s- wave), although there might be longitudinal waves which were still excited. However, in a shear wave, the oscillations are occurring perpendicular to the direction of the wave propagation and consequently the wave velocity is slower than p-wave. Thus, the major portion of energy in s-wave which contains maximum amplitude arrives later than the first p-wave arrivals leading to longer Rise time. Consequently, shear failure shows higher RA value than flexural failure, whereas flexural failure exhibit higher average frequency. In addition, the AE signal frequency could be shifted due to damage and it could be justified by a fundamental concept of physics which is known as the pendulum principle [29].

By using the above descriptions, structural condition evaluation and cracks and failure classification were performed by using transducers mounted on the specimen through recording transient response induced by cracking events. Figure 11 shows failure type classification based

on average frequency versus RA of the beam specimens. The classification of failure type can be performed through separating flexural and shear sources using predefined diagonal lines in the figures which were defined based on the results presented in JCMS for AE monitoring. [29]. It is noteworthy that the presented diagonal lines in Figure 11 are a rough illustration and for each particular material this diagonal line should be obtained to give a precise coordination of this line. As depicted, data were located above the diagonal line for the flexural crack cases and shear sources data were positioned below the diagonal line [19, 29]. Figure 11.a shows the total data during the testing and clearly demonstrates the differences in mode of damage in the GPC, composite and OPC beams where dominant flexural mode of GPC transferred to shear mode in OPC beam. Figures 11.b-e shows loading profile data in 25% segments to show the difference in damage mode over time. As observed, until 50% of the loading profile, flexural mode of damage was the dominant case for all the specimens. However, when the beams were subjected to 40-60 kN, the composite and OPC tended to shear damage. This shear mode was kept in OPC although the composite beam changed to the flexural mode by further loading. The recorded shear transient response at the composite between 50-75% loading profile, Figure 11.f, was attributed to the formation of the horizontal shear cracks at the interface of the specimen although excluding that effect the response of the specimen was flexural as appeared dominant in the last stage profile.

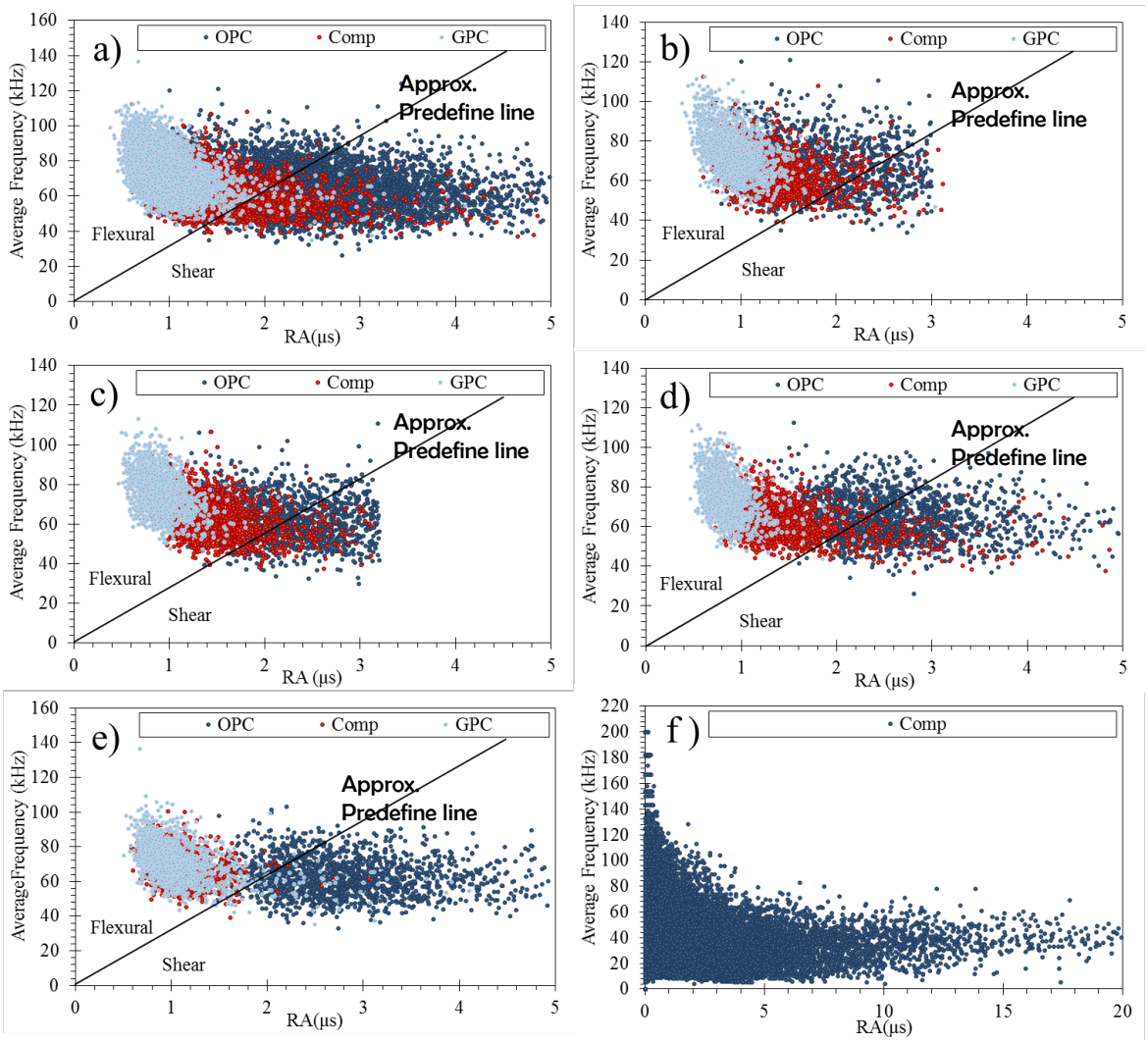

Fig. 11. Failure type classification based on average frequency versus RA. a) Entire data set, b) 25% of loading profile, c) 25-50% of loading profile, d) 50-75% of loading profile, e) 75-100% of loading profile, f) 25-50% of loading profile for composite beam.

3.6. Predictions of flexural strength by ACI 318-14

According to ACI 318-14 and theory of elasticity, the moment strength of first flexural crack, *Mcr*, of the beam specimens are as follows:

$$Mcr = \frac{fct.Ig}{y} \quad (1)$$

where *fct*, *Ig* and *y* are tensile strength, moment of inertia and centroidal axis depth of the gross uncracked-transformed section, respectively.

The ultimate moment strength *Mn* of the beams can be calculated by the following equation:

$$Mn = 0.85.f'c.a.bw.\left(c - \frac{a}{2}\right) + fy.As.(d - c) \quad (2)$$

where $a=\beta_1.c$ is the depth of the equivalent rectangular stress block, β_1 is the factor for the depth of the equivalent stress block, *bw* is the section width, *c* is the neutral axis depth; and *fy*, *As* and *d* are the yielding strength, area and depth of the longitudinal tensile reinforcement, respectively. ACI 318-14 specifies the factor β_1 as below:

$$\beta 1 = 0.65 \leq 0.85 - 0.007(f'c - 28) \leq 0.85 \quad (3)$$

Table 4. Prediction of cracking and ultimate moment using ACI 318-14

Specimens	Mcr (kN.m)			Mmax (kN.m)			Theoretical interface stress (MPa)	
	Exp	ACI 318-14	ACI/Exp	Exp	ACI 318-14	Ratio	Before cracking	After cracking
B1	5.63	4.80	0.85	20.09	17.20	0.86		
B2	6.75	5.90	0.87	21.34	17.20	0.81	0.4	1.3
B3	7.88	5.50	0.70	22.13	17.20	0.78	0.5	1.3
B4	5.43	4.50	0.83	22.09	17.20	0.78	0.5	1.3
B5	4.50	4.80	1.07	20.03	16.60	0.83		

Table 4 compares the experimental values of Mcr and Mmax versus the numerical values calculated by ACI 318-14. Although the cracking moment of both GPC and OPC specimens was predicted properly, the composite beams showed higher resistance against the applied moment to cracking. This enhancement is attributed to the higher stiffness of the beams because of the large concrete section at the top and the GPC section with higher degree of plasticity at the tensile zone of the specimens. Therefore, these specimens not only had larger curvature but could also resist more plastic strain leading to postponement of the first crack occurrence. On the other hand, the maximum moment strength predicted by ACI 318-14 had almost similar accuracy for OPC and GPC beams although as mentioned in the section 3.3, the depth of compressive block at cracked section of GPC was higher in comparison with conventional concrete. Therefore the specified $\beta 1$ factor in ACI 318-14, equation (3), was expected to be specified for GPC to achieve higher degree of accuracy in this calculation. Further, in the case of composite beams, since the crack propagation was limited to the geopolymer section after about 55 kN, it is expected that degree of damage in concrete section of composite specimens was lower than that of the GPC specimen; as a result, they could resist against higher applied moment. In our further study the effect of contact strength on the performance of the OPC/GPC composite beams will be discussed. However, it is notable that both Mcr and Mmax predicted by ACI 318-14 was underestimated in comparison to the recorded experimental result and the specimens had higher degree of moment capacity than these calculations.

4. Conclusion

This study considered the structural response and failure mode of a novel steel reinforced concrete composite beam for precast construction using the benefits of geopolymer concrete at the tensile zone and normal Portland cement based concrete at the compression zone of the beam specimens. Based on the experimental results of mechanical and acoustic emission analysis, the following conclusions were drawn:

The GPC beams shows higher ductility and toughness relative to the OPC specimens without an adverse effect on its ultimate load carrying capacity. Further, tensile zone replacement of the OPC beam by a geopolymer section resulted in energy absorption enhancement and improved their ultimate load resistance. The first cracking moment of the composite beams was significantly increased in comparison to either OPC or GPC specimens owing to the presence of large portion of the OPC section at the top which provided the stiffness while GPC at the bottom had higher uncracked strain capacity than OPC.

The pattern of crack propagation was different in composite specimens than either OPC or GPC beams. Moreover, after formation of horizontal shear cracks, formation of new cracks were limited to the geopolymer section. However, the fracture and damage zone in geopolymer and composite beams were larger than GPC beam. In addition, from the AE results, it was observed that shear mode of damage and failure of the OPC beams were transferred to the flexural mode in the composite and GPC specimens.

The experimental cracking and ultimate cracking were predicted by ACI 318-314 with some expected discrepancies. However it is expected that β_1, which is the factor for the depth of the equivalent stress block, could be characterized for geopolymer concretes in further studies to improve the design accuracy of the geopolymer beams.

5. Acknowledgement

This research work was funded by the University of Malaya under High Impact Research Grant (HIRG) No. UM.C/HIR/MOHE/ENG/02/D000002-16001 (synthesis of blast resistant structures). We would also like to acknowledge the contribution of Ms Marya Bagherifaez, and Mr. Sreedharan from the Department of Civil Engineering at University of Malaya.

References

[1] T. Roberts, Finite difference analysis of composite beams with partial interaction, Computers & structures 21(3) (1985) 469-473.
[2] K. Elliott, Precast concrete structures, Elsevier2002.
[3] J.M. Gere, B.J. Goodno, Mechanics of Materials, 8e, (1984).
[4] K. MACKENZIE, M. WELTER, Geopolymer (aluminosilicate) composites: synthesis, properties and applications, Advances in Ceramic Matrix Composites (2014) 445.
[5] J. DAVIDOVITS, Geopolymer Chemistry and Applications, 3rd ed., Institut Géopolymère2008.
[6] P. Duxson, Geopolymer precursor design, Geopolymers: Structures, Processing, Properties and Industrial Applications (2009) 37.
[7] N. Ranjbar, M. Mehrali, U.J. Alengaram, H.S.C. Metselaar, M.Z. Jumaat, Compressive strength and microstructural analysis of fly ash/palm oil fuel ash based geopolymer mortar under elevated temperatures, Construction and Building Materials 65(0) (2014) 114-121.
[8] M. Saafi, K. Andrew, P.L. Tang, D. McGhon, S. Taylor, M. Rahman, S. Yang, X. Zhou, Multifunctional properties of carbon nanotube/fly ash geopolymeric nanocomposites, Construction and Building Materials 49 (2013) 46-55.
[9] N. Ranjbar, M. Mehrali, M. Mehrali, U.J. Alengaram, M.Z. Jumaat, Graphene nanoplatelet-fly ash based geopolymer composites, Cement and Concrete Research 76 (2015) 222-231.
[10] J. Aldred, J. Day, Is geopolymer concrete a suitable alternative to traditional concrete, 37th Conference on our world in concrete & structures, CI-PREMIER PTE LTD,(29-31 August 2012), Singapore, 2012.
[11] VicRoads, General Concrete Paving, Section 703, Victoria-Australia, 2010.
[12] J.L. Provis, J.S. van Deventer, Alkali Activated Materials: State-of-the-art Report, RILEM TC 224-AAM, Springer Dordrecht2014.
[13] J.L. Provis, Alkali-activated Binders and Concretes: The Path to Standardization, ASTM International, 2013, pp. 185–195.
[14] D.G.B. Jannie S. J. van Deventer, Susan A. Bernal, John L. Provis, Development, Standardization, and Applications of Alkali-activated Concretes, (2013) 196–212.
[15] J. Gourley, G. Johnson, Developments in geopolymer precast concrete, World Congress Ceopolymer, 2005, pp. 139-143.
[16] E.I. Diaz-Loya, E.N. Allouche, S. Vaidya, Mechanical properties of fly-ash-based geopolymer concrete, ACI Materials Journal 108(3) (2011).
[17] A. Behnia, H.K. Chai, T. Shiotani, Advanced structural health monitoring of concrete structures with the aid of acoustic emission, Construction and Building Materials 65(0) (2014) 282-302.

[18] D. Aggelis, D. Soulioti, E. Gatselou, N.-M. Barkoula, T. Matikas, Monitoring of the mechanical behavior of concrete with chemically treated steel fibers by acoustic emission, Construction and Building Materials 48 (2013) 1255-1260.
[19] A. Carpinteri, A. Grazzini, G. Lacidogna, A. Manuello, Durability evaluation of reinforced masonry by fatigue tests and acoustic emission technique, Structural Control and Health Monitoring 21(6) (2014) 950-961.
[20] A. Farhidzadeh, S. Salamone, B. Luna, A. Whittaker, Acoustic emission monitoring of a reinforced concrete shear wall by b-value based outlier analysis, Structural Health Monitoring (2012) 1475921712461162.
[21] W.-F. Chen, Plasticity in reinforced concrete, J. Ross Publishing2007.
[22] R. Andalib, M.W. Hussin, M.Z.A. Majid, M. Azrin, H.H. Ismail, Structural Performance of Sustainable Waste Palm Oil Fuel Ash-Fly Ash Geo-polymer Concrete Beams, Journal of Environmental Treatment Techniques 2(3) (2014) 115-119.
[23] P.K. Sarker, Bond strength of reinforcing steel embedded in fly ash-based geopolymer concrete, Materials and structures 44(5) (2011) 1021-1030.
[24] N. Ranjbar, M. Mehrali, M. Mehrali, U.J. Alengaram, M.Z. Jumaat, High tensile strength fly ash based geopolymer composite using copper coated micro steel fiber, Construction and Building Materials 112 (2016) 629-638.
[25] N. Ranjbar, S. Talebian, M. Mehrali, C. Kuenzel, H.S.C. Metselaar, M.Z. Jumaat, Mechanisms of interfacial bond in steel and polypropylene fiber reinforced geopolymer composites, Composites Science and Technology 122 (2016) 73-81.
[26] M. Gohnert, Proposed theory to determine the horizontal shear between composite precast and in situ concrete, Cement and Concrete Composites 22(6) (2000) 469-476.
[27] K. Haidar, G. Pijaudier-Cabot, J.-F. Dubé, A. Loukili, Correlation between the internal length, the fracture process zone and size effect in model materials, Materials and structures 38(2) (2005) 201-210.
[28] P. Rossi, J. Robert, J. Gervais, D. Bruhat, The use of acoustic emission in fracture mechanics applied to concrete, Engineering Fracture Mechanics 35(4) (1990) 751-763.

Table
Click here to download Table: Tables.docx

Table 1. XRF analysis of the Fly ash and Portland cement

Oxide composition	Fly ash (%)	Portland cement (%)
SiO_2	75.76	16.68
Al_2O_3	15.86	4.41
Fe_2O_3	3.90	3.64
K_2O	1.14	0.37
TiO_2	0.97	0.17
CaO	0.95	68.36
SO_3	0.35	4.80
MgO	0.26	1.29
P_2O_5	0.21	0.05
Na_2O	0.16	-
ZrO_2	0.13	-
MnO	0.06	0.10

Table 2. Mechanical properties of the Portland cement based and geopolymer concrete.

	Compressive strength, f_c (MPa)	Tensile strength*, f_{ct} (MPa)	Young's modulus, E (GPa)
Geopolymer concrete	42±3	5.2±0.3	22.4±1
High strength concrete	88±5	5.5±0.2	40.5+2

*Similar tensile strength is considered for the OPC and GPC since the tensile zone of the beams are replaced.

Table 3. Crack properties of the beams

Specimens	Depth of GPC layer (mm)	First crack Load (kN)	First crack length (cm)	Crack length (cm)			
				Load ≤60kN (cm)	Load>60kN (cm)	Total crack length until yielding (cm)	Before/after 60kN (cm)
B1	0	25	7	75	13	88	5.8
B2	50	30	12.5	89	33	122	2.7
B3	75	35	13	104	58	162	1.8
B4	100	30	9	76	40	116	1.9
B5	200	20	7	81	63	144	1.3

Table 4. Prediction of cracking and ultimate moment using ACI 318-14

Specimens	Mcr (kN.m)			Mmax (kN.m)			Theoretical interface stress (MPa)	
	Exp	ACI 318-14	ACI/Exp	Exp	ACI 318-14	Ratio	Before cracking	After cracking
B1	5.63	4.80	0.85	20.09	17.20	0.86		
B2	6.75	5.90	0.87	21.34	17.20	0.81	0.4	1.3
B3	7.88	5.50	0.70	22.13	17.20	0.78	0.5	1.3
B4	5.43	4.50	0.83	22.09	17.20	0.78	0.5	1.3
B5	4.50	4.80	1.07	20.03	16.60	0.83		

Figure
Click here to download Figure: Figures.docx

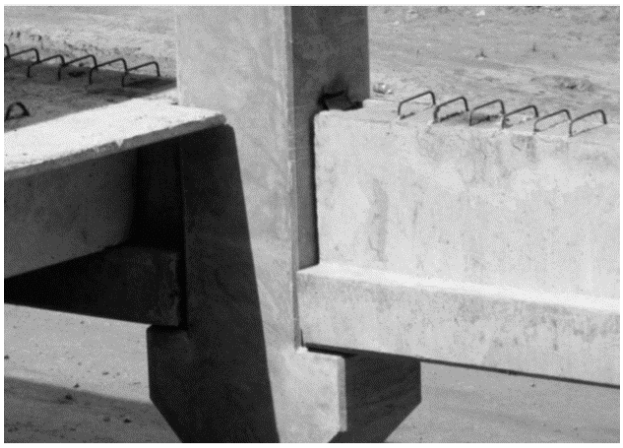

Fig. 1. Application of multi-layers composite inverted T-beam [3].

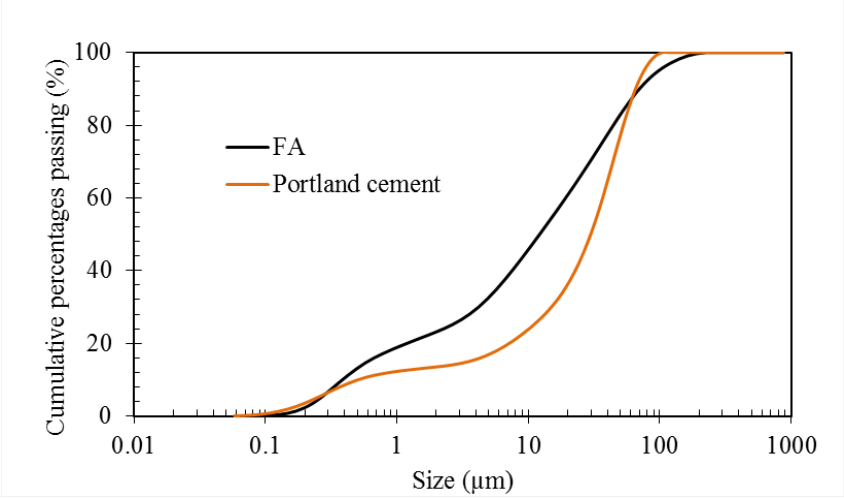

Fig. 2. Particle size distribution of the fly ash and Portland cement.

Fig. 3. Casting of different layers and final beam products.

2.3.

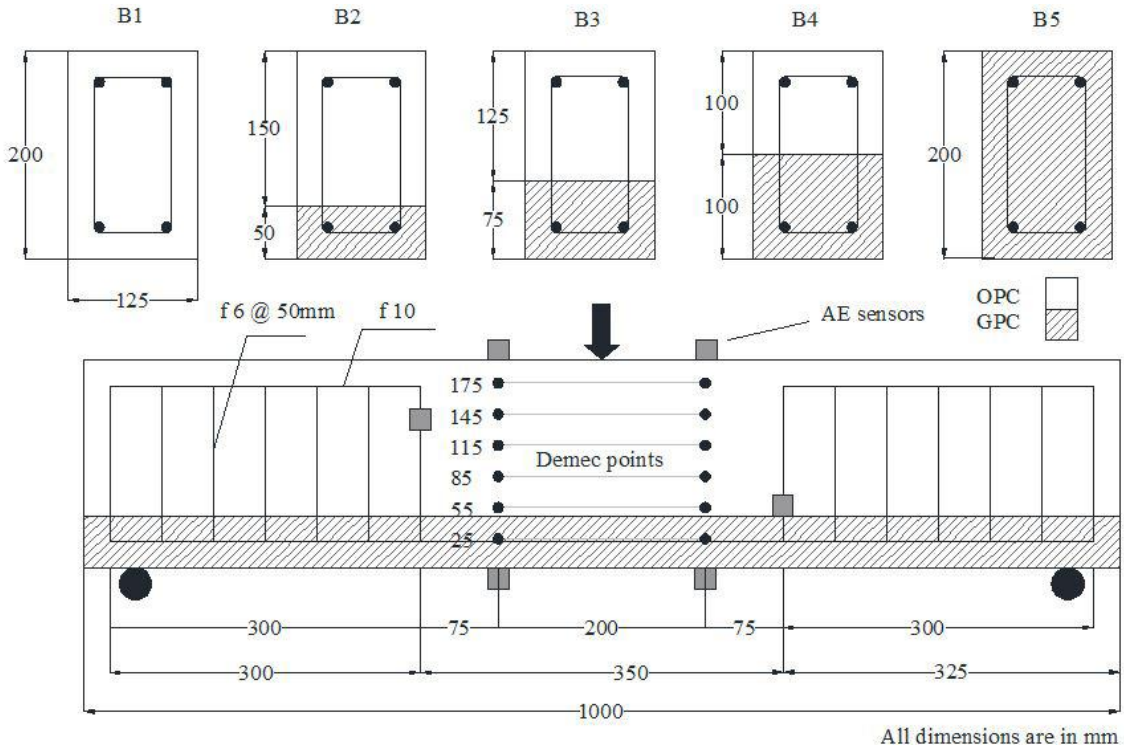

Fig. 4. Geometry of the multilayers steel reinforced GPC/OPC composite beams.

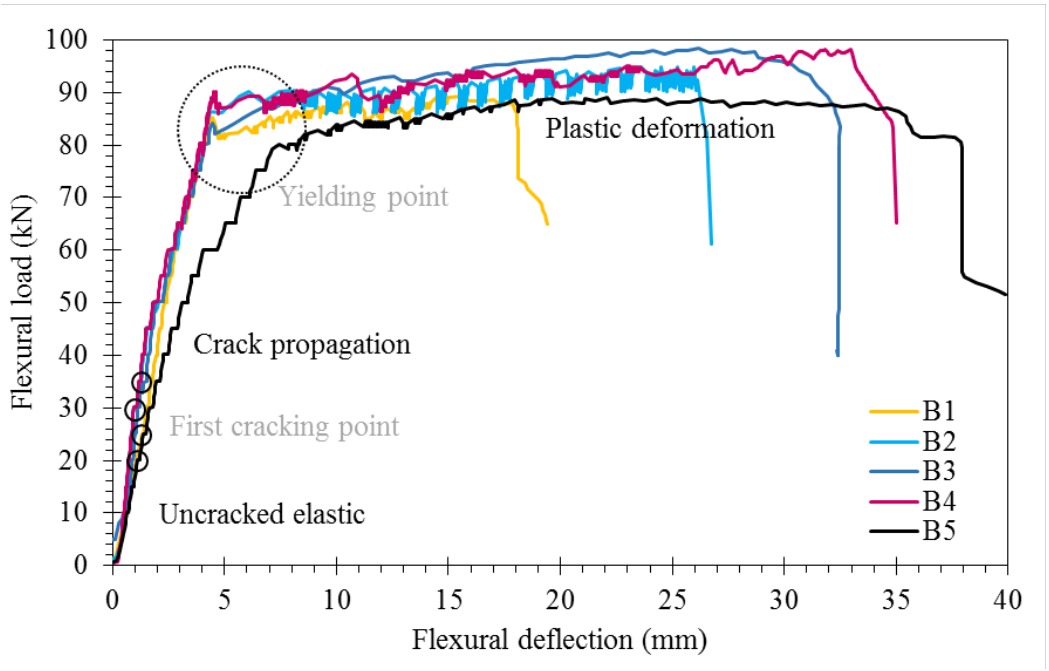

Fig. 5. Load-deflection curves of multilayer GPC/OPC steel reinforced concrete beams.

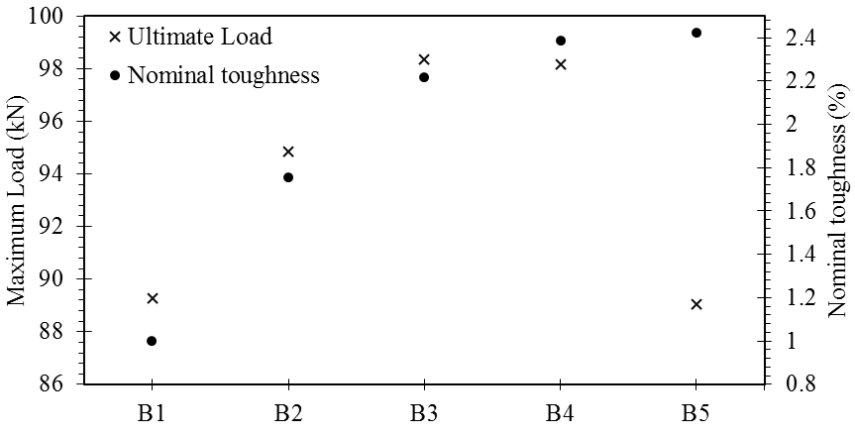

Fig. 6. Maximum load capacity and nominal toughness of the geopolymer composite beams.

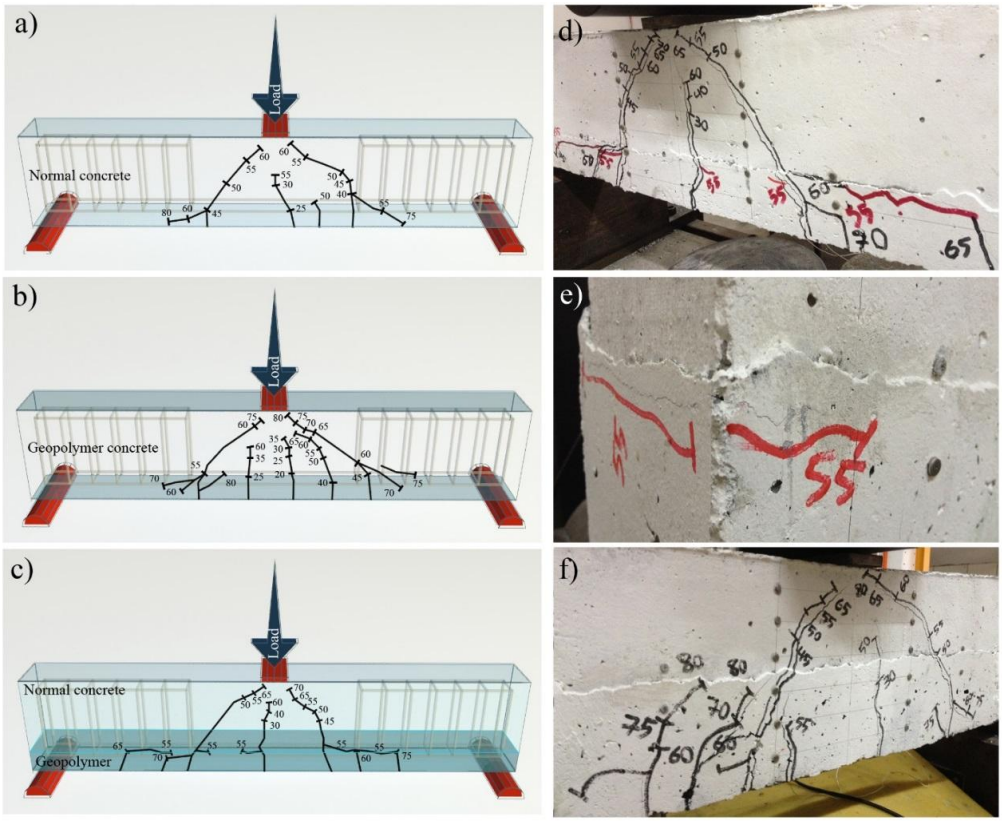

Fig. 7. Scheme of Crack patterns in a) OPC beam, b) GPC beam, c) composite beam-B2, d) experimental crack pattern of B2, e) horizontal shear force at the end of the B3, f) crack pattern of B4.

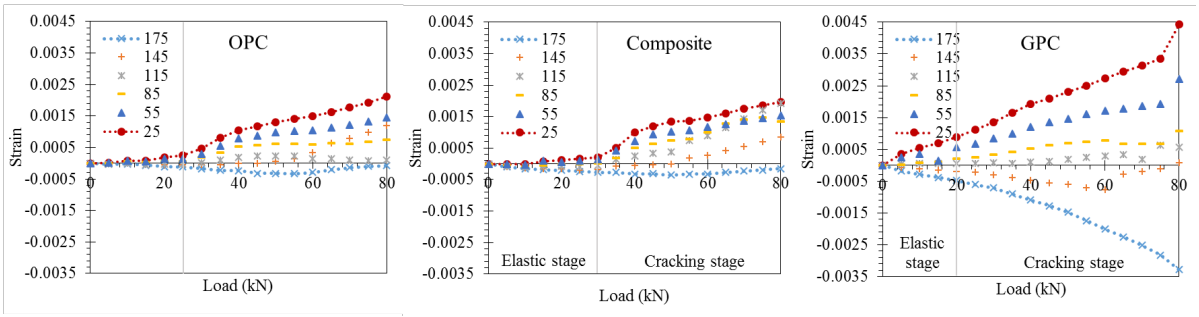

Fig. 8. Strain variation along the depth of the section over load. The legend shows the location of demec-points according to the Figure.4.

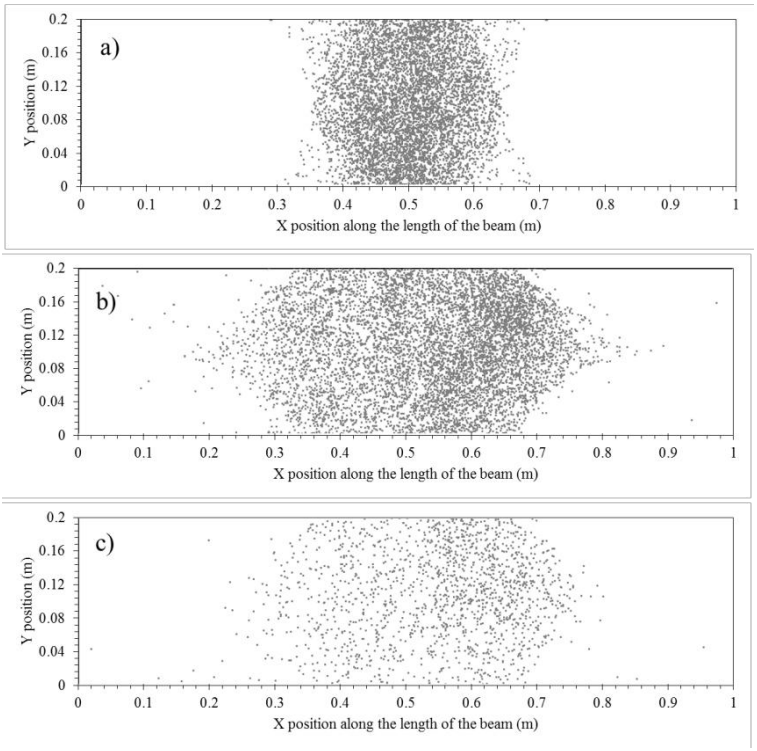

Fig. 9. 2D AE event localization of the a) OPC, b) Composite, c) GPC beam.

.

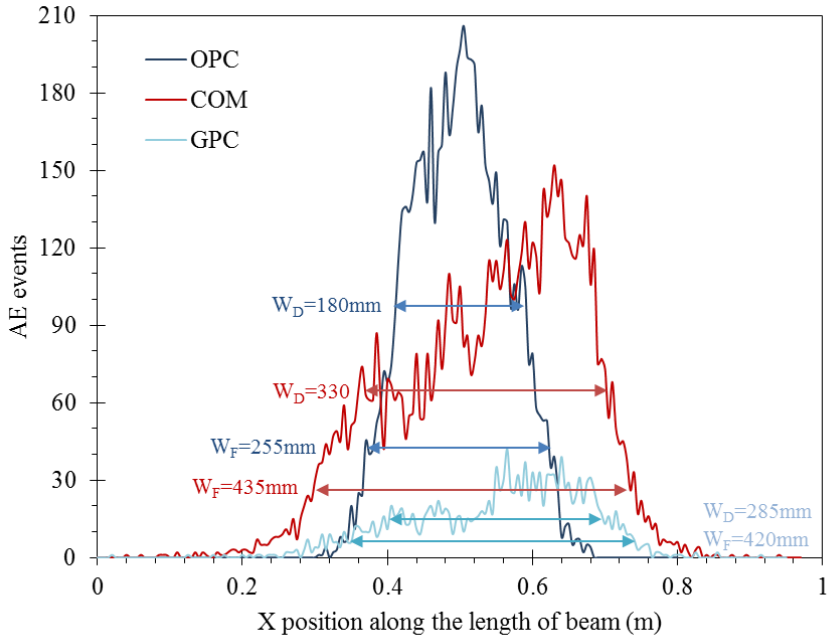

Fig. 10. AE-events versus specimen length.

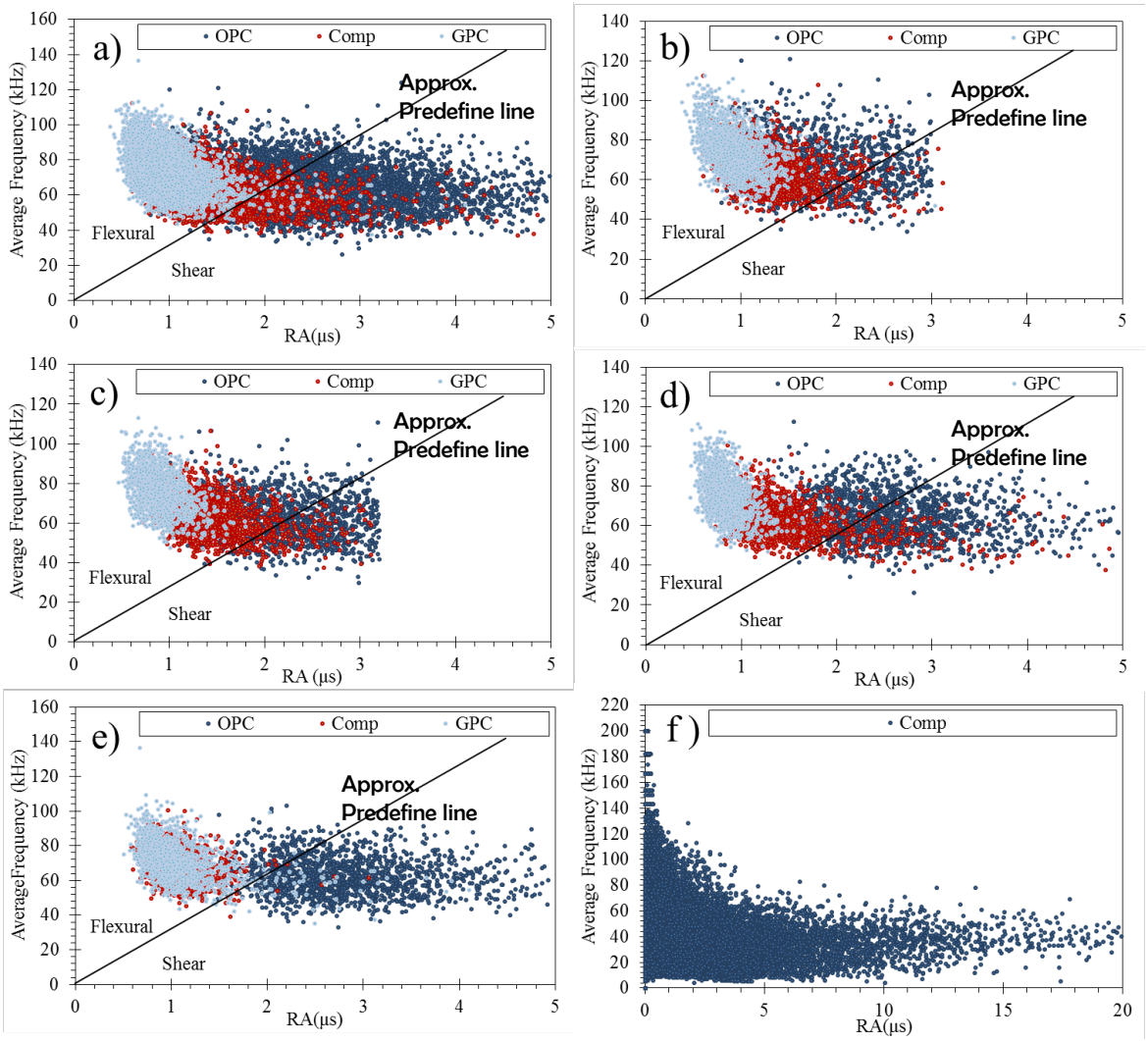

Fig. 11. Failure type classification based on average frequency versus RA. a) Entire data set, b) 25% of loading profile, c) 25-50% of loading profile, d) 50-75% of loading profile, e) 75-100% of loading profile, f) 25-50% of loading profile for composite beam.